Direct-forcing immersed-boundary method: a simple correction preventing boundary slip error

Simon Gsell, Julien Favier

Direct-forcing immersed-boundary method: a simple correction preventing boundary slip error

Simon Gsell[a,b,*], Julien Favier[b]

[a]Aix Marseille Univ, Université de Toulon, CNRS, CPT, Turing Center for Living Systems, Marseille, France
[b]Aix Marseille Univ, CNRS, Centrale Marseille, M2P2, Marseille, France

Abstract

The boundary slip error resulting from the interpolation/spreading non-reciprocity of the direct-forcing immersed-boundary method is analyzed based on a simple and generic theoretical framework. In explicit implementations, the slip error scales with the Courant number, as predicted by the analysis and confirmed by lattice-Boltzmann simulation results. Using an analytical approximation of the non-reciprocity error, the immersed-boundary force can be corrected in order to prevent boundary slip and flow penetration. This *a priori* correction leads to a major improvement of the no-slip condition while avoiding any additional computational time or implementation effort.

1. Introduction

The immersed-boundary (IB) method is a popular approach to model fluid flows around curved, moving and/or deformable solid walls. First introduced by Peskin [1], the method has motivated a number of developments and has been applied to a variety of fluid flow problems [2, 3]. The key concept of the method relies on the introduction of a space/time-dependant body force in the flow momentum equation, enforcing the no-slip condition on the wall. Different strategies have been proposed concerning the transfer of information between the boundary and the fluid volume or regarding the computation of the IB force, leading to the vast family of IB methods that one knows nowadays.

Among these methods, the direct-forcing approach is widely employed for configurations involving solid or flexible walls [4, 5, 6, 7, 8, 9]. In the time-discretized equations, the IB force is generally determined on the immersed boundary after the interpolation of a prediction flow velocity. The forcing is then distributed over the fluid volume using the same interpolation kernel, an operation referred to as *spreading*. However, this explicit procedure can lead to boundary slip and flow penetration, depending on the numerical and physical parameters [10]. Several strategies have been proposed to overcome this problem, such as multi-direct-forcing methods [10] and implicit IB methods [9, 11, 12]. While these methods are effective in correcting the slip error of the IB method, they involve additional computational cost and/or implementation effort. In addition, a general theoretical analysis addressing the origin of these errors is still missing.

In this brief note, we use simple theoretical arguments to quantify the IB error in terms of non-reciprocity between the interpolation and spreading operators. Our analysis allows us to propose a generic correction of the direct-forcing scheme that takes the form of a rescaled IB forcing. The method is implemented in a lattice-Boltzmann code and applied to relevant test cases. The boundary slip predicted *a priori* is accurately reproduced in the numerical tests. A major decrease of these errors is obtained when the corrected scheme is employed.

2. Theoretical analysis

In the two-dimensional (x, y) frame, consider the incompressible IB problem governed by the momentum equation

$$\rho \frac{\partial \boldsymbol{u}(\boldsymbol{x}, t)}{\partial t} = \nabla \cdot \boldsymbol{\mathcal{F}}(\boldsymbol{x}, t) + \mathcal{S}[\boldsymbol{G}](\boldsymbol{x}, t), \tag{1}$$

*Corresponding author, simon.gsell@univ-amu.fr

where $\boldsymbol{x}$ is the position vector in the fluid volume Ω, $\boldsymbol{u}$ is the flow velocity, t is time, $\mathcal{F}$ represents the momentum fluxes of the Navier-Stokes momentum equation, $\boldsymbol{G}$ is the IB force defined on the immersed boundary Γ and $\mathcal{S}$ is the spreading operator distributing the force $\boldsymbol{G}$ over a small fluid volume around Γ. Any position on the immersed boundary is represented by $\boldsymbol{X}(r,t)$, where r is a curvilinear coordinate. The spreading process is performed using a regularized Dirac function $\delta(\boldsymbol{x})$, namely

$$\mathcal{S}[\boldsymbol{G}](\boldsymbol{x}) = \int_{\Gamma} \boldsymbol{G}(r)\delta(\boldsymbol{x} - \boldsymbol{X}(r))\Delta S\,(r)dr, \tag{2}$$

where ΔS is a characteristic width of the boundary, that is typically set to 1, in mesh units. The same kernel function is used to define the interpolation operator,

$$\mathcal{I}\left[\phi\right](r) = \int_{\Omega} \phi(\boldsymbol{x})\delta(\boldsymbol{x} - \boldsymbol{X}(r))dxdy, \tag{3}$$

which is used to compute a representative value of any quantity ϕ on the boundary.

The procedure employed to determine $\boldsymbol{G}$ is described in the time-discrete space. Time is discretized as $t^n = n\Delta t$, where Δt is the time step. In many explicit IB implementations, the time-stepping procedure is decomposed into two steps [9]. First, a prediction flow velocity $\boldsymbol{u}^*$ is computed in the absence of IB forcing. Then, $\boldsymbol{u}^*$ is interpolated on the immersed boundary using equation (3), and the IB force is defined as

$$\boldsymbol{G} = \frac{\rho}{\Delta t^*}\left(\boldsymbol{U_b} - \mathcal{I}[\boldsymbol{u}^*]\right), \tag{4}$$

where $\boldsymbol{U_b}$ is the prescribed boundary velocity and Δt^* denotes an IB time step that depends on the employed numerical scheme. Several strategies can be used to update the flow velocity as a function of $\boldsymbol{G}$. Here, the IB properties are illustrated on the basis of a simple explicit time integration, namely

$$\boldsymbol{u}^{n+1} = \boldsymbol{u}^* + \frac{\Delta t^*}{\rho}\mathcal{S}[\boldsymbol{G}]. \tag{5}$$

The boundary slip resulting from the above model algorithm is determined hereafter. According to equation (5), the interpolated velocity reads

$$\mathcal{I}\left[\boldsymbol{u}^*\right] = \mathcal{I}[\boldsymbol{u^{n+1}}] - \frac{\Delta t^*}{\rho}\mathcal{I}\left[\mathcal{S}[\boldsymbol{G}]\right]. \tag{6}$$

As detailed in Ref. [13], the re-interpolation operator in (6) can be approximated as $\mathcal{I}\left[\mathcal{S}[\boldsymbol{G}]\right] \approx \kappa\boldsymbol{G}$, where $\kappa = \int \delta(x)^2 dx$ only depends on the employed regularized Delta function. This analytical approximation is based on the following assumptions: (i) the curvature of Γ is small enough so that it can be locally represented by a straight wall and (ii) the variation of $\boldsymbol{G}$ along the boundary remains small. Combining (4) and (6), the velocity slip on the boundary can be expressed as $\boldsymbol{U_b} - \mathcal{I}[\boldsymbol{u}^{n+1}] = (1-\kappa)\boldsymbol{G}\Delta t^*/\rho$. Therefore, the boundary slip vanishes if $\kappa = 1$, i.e. if the interpolation and spreading operators are reciprocal; however, since $\kappa < 1$ for usual kernel functions [13], a substantial boundary slip typically emerges. Even though its detailed expression may depend on the time integration scheme, such interpolation/spreading error is generally expected in IB methods. In order to satisfy the hydrodynamic similarity principle, the magnitude of the IB force must scale as $\sim \rho U_0^2/\Delta n$, where U_0 is the reference flow velocity and Δn is the typical grid spacing. Consequently, in the present model algorithm, the normalized velocity-slip error magnitude $|\boldsymbol{E}| = |\boldsymbol{U_b} - \mathcal{I}[\boldsymbol{u}^{n+1}]|/U_0$ is expected to vary as

$$|\boldsymbol{E}| \sim U_0\Delta t^*/\Delta n, \tag{7}$$

i.e. the non-dimensional velocity slip scales with the Courant number $C = U_0\Delta t^*/\Delta n$.

In order to enforce the no-slip condition on the boundary, the magnitude of the IB force can be corrected by introducing a non-dimensional scaling coefficient γ, namely $\boldsymbol{G^*} = \gamma\boldsymbol{G}$. Using expressions (4)-(6), the correction coefficient can be expressed as

$$\gamma = \frac{\Delta t^* G^{*2}}{\rho\left(\boldsymbol{U_b} - \mathcal{I}[\boldsymbol{u^{n+1}}]\right)\cdot\boldsymbol{G^*} + \kappa\Delta t^* G^{*2}}, \tag{8}$$

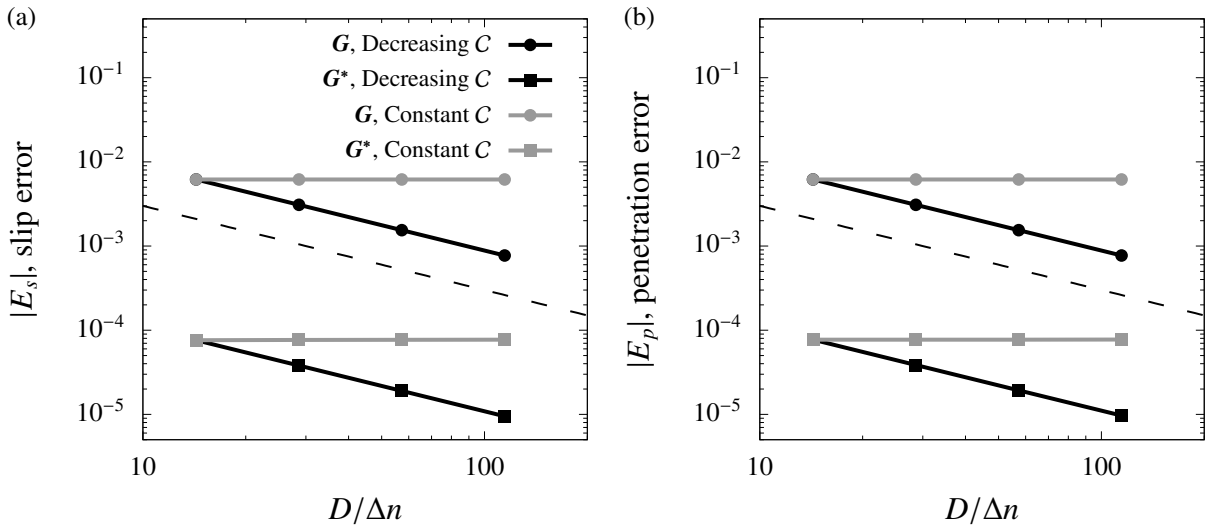

Figure 1: Evolution of the (a) slip and (b) penetration errors on a straight immersed boundary, for the standard (4) and corrected (9) IB forces, $\boldsymbol{G}$ and $\boldsymbol{G}^*$. The dashed line indicates the trend $(D/\Delta n)^{-1}$.

where $G^{*2} = |\boldsymbol{G}^*|^2$. If the no-slip condition $\mathcal{I}[\boldsymbol{u}^{n+1}] = \boldsymbol{U_b}$ is satisfied, the correction coefficient reduces to $1/\kappa$. Therefore, the corrected IB force should be expressed as

$$\boldsymbol{G}^* = \frac{\rho}{\kappa \Delta t^*} \left(\boldsymbol{U_b} - \mathcal{I}[\boldsymbol{u}^*] \right). \tag{9}$$

The corrected direct-forcing algorithm is then obtained by substituting $\boldsymbol{G}$ by $\boldsymbol{G}^*$ in Eq. (5). Note that, even if a model temporal algorithm has been used in the present analysis, the expression of $\boldsymbol{G}^*$ is not related to any specific temporal scheme, as it generally ensures $\mathcal{I}[\mathcal{S}(\boldsymbol{G}^*)] \approx \boldsymbol{G}$, correcting the boundary slip error emerging from interpolation/spreading non-reciprocity. Expression (9) can be thought as an explicit analytical approximation of the implicit IB corrections [9, 12] that otherwise require the resolution of a linear system to enforce the interpolation/spreading reciprocity condition. As shown in the following, this *a priori* correction allows to drastically decrease the numerically-observed boundary slip error.

3. Numerical results

The corrected IB scheme (9) is implemented in a two-relaxation-time lattice-Boltzmann code coupled to a direct-forcing IB method. It is recalled that the analysis proposed in §2 is generic, since the choice of the fluid-flow solver mainly impacts the computation of the prediction velocity $\boldsymbol{u}^*$, while the direct-forcing immersed-boundary algorithm remains mostly similar from one method to the other. Here, the lattice-Boltzmann method is thus employed only as an example of numerical method for the resolution of the Navier-Stokes equations. Details on the present algorithm are provided in Refs. [13, 14]. Note that the present implementation is equivalent to the time-stepping procedure described by Eqs. (4)-(5), with $\Delta t^* = \Delta t/2$. The employed Dirac function corresponds to $\kappa = 1/2$; values of κ for various usual functions are provided in Ref. [13]. It is worth mentioning that the modification of the IB force magnitude in equation (9) may alter the stability of the computations, depending on the physical configuration and numerical parameters. This effect is expected due to the increased stiffness of the corrected method: since $\kappa < 1$ in Eq. (9), the IB force magnitude generally tends to be locally higher when using the corrected scheme. The resulting numerical stability might be flow-solver dependent. In the present simulations, this effect was mostly observed during the first time steps after uniform-flow initializations, where significant oscillations of the IB force were observed. In order to stabilize and accelerate the flow transition from initial conditions, these oscillations have been damped by relaxing the IB force during the first time steps as $\boldsymbol{G}^{n+1} = \beta \boldsymbol{G}^* + (1-\beta)\boldsymbol{G}^n$, with β a relaxation parameter set to 0.6.

A simple test case is proposed to illustrate the theoretical analysis developed in §2. In a periodic computational domain, a straight immersed boundary extends from the bottom left corner to the top right corner of the domain,

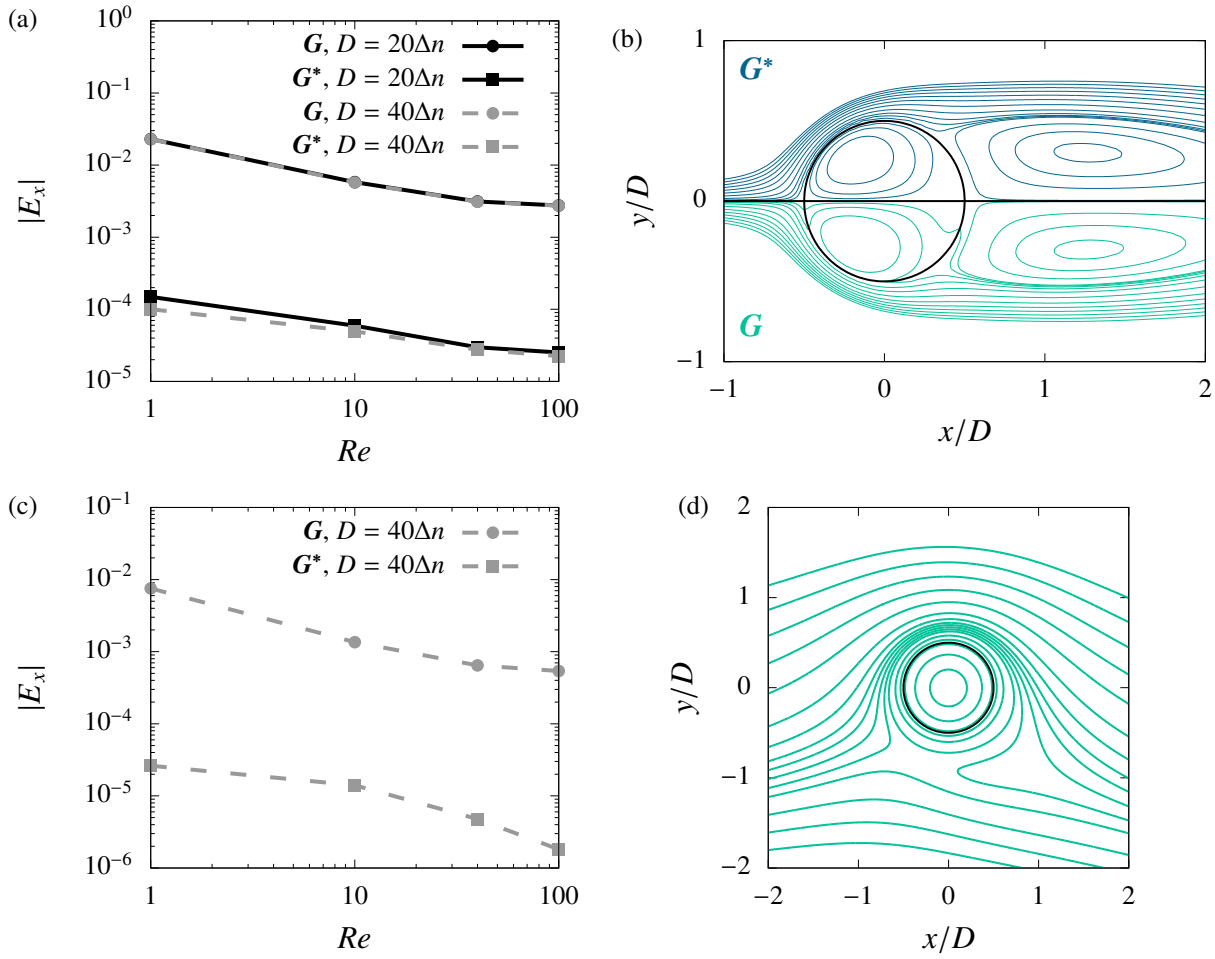

Figure 2: (a,b) Velocity error on a cylinder immersed in a flow: (a) evolution of the streamwise velocity error as a function of Re and $D/\Delta n$ and (b) flow streamlines below/above the symmetry plane at $Re = 40$ and $D = 40\Delta n$, for the standard (4) and corrected (9) IB forces, $\boldsymbol{G}$ and $\boldsymbol{G}^*$. (c,d) Velocity error on a rotating cylinder, for $\alpha = 3$ and $D/\Delta n = 40$: (c) evolution of the streamwise velocity error as a function of Re and (d) streamlines near the cylinder obtained using the corrected IB force $\boldsymbol{G}^*$ (9) at $Re = 40$.

reproducing a channel flow configuration. The flow is driven by a body force $\boldsymbol{g}$, whose direction can be either parallel (leading to Poiseuille flow) or normal (leading to hydrostatic equilibrium) to the wall, i.e. $\boldsymbol{g} = |\boldsymbol{g}|\boldsymbol{t}$ or $\boldsymbol{g} = |\boldsymbol{g}|\boldsymbol{n}$, where $(\boldsymbol{t}, \boldsymbol{n})$ is the frame aligned with the channel direction. The angle between $\boldsymbol{t}$ and $\boldsymbol{x}$, denoted by θ, is set to $\theta \approx 25°$ in this example (i.e. avoiding singular cases as $\theta = 0°$ or $\theta = 45°$). The reference velocity is set to $U_0 = \sqrt{|\boldsymbol{g}|D}$, where D is the channel width, and the Reynolds number is $Re = U_0 D/\nu \approx 2$, with ν the kinematic viscosity.

The evolution of the average slip error $E_s =< \boldsymbol{E} \cdot \boldsymbol{t} >$, where <> denotes the averaging over the IB markers and $\boldsymbol{E}$, defined in §2, is determined numerically by interpolating the corrected fluid velocity on the immersed boundary, is analyzed in the case $\boldsymbol{g} = |\boldsymbol{g}|\boldsymbol{t}$ and depicted in figure 1(a). The mesh-unit channel width is varied while keeping the Reynolds number constant, by varying either the mesh-unit velocity (i.e. Courant number) $U_0\Delta t/\Delta n \sim (D/\Delta n)^{-1}$ or the mesh-unit fluid viscosity $\nu\Delta t/\Delta n^2 \sim D/\Delta n$. As predicted by equation (7), a first-order mesh convergence is obtained when the Courant number C is varied together with $D/\Delta n$; in contrast, the velocity error remains unchanged when C is kept constant. For a given grid spacing, the slip error is decreased by two orders of magnitude when the corrected IB scheme is used. The penetration error $E_p =< \boldsymbol{E} \cdot \boldsymbol{n} >$ exhibits the same evolution when $\boldsymbol{g} = |\boldsymbol{g}|\boldsymbol{n}$ (figure 1(b)), supporting that the boundary error varies as a function of $\boldsymbol{G}$ (whose magnitude is prescribed by the external body force here) and does not depend on the flow details.

The present method is then applied to a circular cylinder of diameter D immersed in an oncoming flow with

velocity $U_0\boldsymbol{x}$, as a typical configuration involving curved geometries, stagnation points, shear flows and possibly detached and unsteady flows, depending on the Reynolds number. Velocity and pressure Dirichlet conditions are set at the inlet and outlet of the domain, located at a distance of $20D$ upstream and $40D$ downstream of the body. Periodic conditions are set at the two other boundaries, placed 20 diameters away from the cylinder. The flow velocity is fixed to $U_0 = 0.05\Delta n/\Delta t$ to ensure optimal numerical accuracy and efficiency, i.e. the Courant number is kept constant. The previously-observed IB properties are confirmed in the present configuration: on the considered range of Reynolds numbers, the streamwise velocity error $E_x =< \boldsymbol{E} \cdot \boldsymbol{x} >$ is hardly affected by the grid spacing and it is decreased by two orders of magnitude by the corrected direct-forcing method, as depicted in figure 2(a) and illustrated by the streamlines in figure 2(b). When the corrected method is used, the boundary error tends to decrease as a function of $D/\Delta n$, as expected since the estimation of κ is based on a plane-boundary approximation. It is shown however that these variations are small compared to the difference of accuracy between the standard and corrected IB forces. The fluid forces are also accurately predicted by the corrected method. At $Re = 100$ and $D/\Delta n = 40$, the non-dimensional vortex-shedding frequency, time-averaged drag coefficient and peak lift coefficient are equal to 0.164, 1.37 and 0.34, in agreement with the values 0.164, 1.32 and 0.32 issued from the high-resolution simulations performed by Bourguet and Lo Jacono [15].

Finally, the rotating cylinder is considered as a typical test case involving non-zero boundary velocities. The rotation rate $\alpha = \omega D/2U_0$, with ω the angular velocity of the cylinder, is fixed to 3, the inflow velocity is set to $U_0 = 0.05/\alpha$, and the cylinder diameter is $D/\Delta n = 40$. Figure 2(c) shows the evolution of the streamwise velocity error as a function of the Reynolds number. The substantial improvement provided by the corrected scheme is also clearly noted in this case, as the velocity error is globally decreased by two orders of magnitude by the corrected method. The flow streamlines, plotted in figure 2(d) for the corrected-IB simulation at $Re = 40$, are well-aligned with the cylinder surface and in good agreement with previously reported flow patterns [16].

4. Summary

Using a general theoretical framework, we have emphasized the existence of a boundary slip error intrinsic to the direct-forcing IB method and emerging from the non-reciprocity of the interpolation and spreading operators. When a simple explicit time integration is employed, the resulting slip error scales with the Courant number, as predicted by the theory and accurately confirmed by lattice-Boltzmann simulation results. This error, whose exact magnitude may depend on the implemented numerical schemes, can however be corrected through a simple and generic *a priori* correction of the IB force, without any additional computational time or implementation effort.

Acknowledgements

S. G. has received funding from the SINUMER project (ANR-18-CE45-0009-01) of the French National Research Agency (ANR).

References

[1] C. S. Peskin, The immersed boundary method, Acta Numerica 11 (2002) 479517.
[2] R. Mittal, G. Iaccarino, Immersed boundary methods, Annual Review of Fluid Mechanics (2004) 24.
[3] W. Kim, H. Choi, Immersed boundary methods for fluid-structure interaction: A review, International Journal of Heat and Fluid Flow.
[4] E. Fadlun, R. Verzicco, P. Orlandi, J. Mohd-Yusof, Combined immersed-boundary finite-difference methods for three-dimensional complex flow simulations, Journal of Computational Physics 161 (1) (2000) 3560.
[5] J. Kim, D. Kim, H. Choi, An immersed-boundary finite-volume method for simulations of flow in complex geometries, Journal of Computational Physics 171 (1) (2001) 132150.
[6] E. Balaras, Modeling complex boundaries using an external force field on fixed Cartesian grids in large-eddy simulations, Computers & Fluids 33 (3) (2004) 375404.
[7] M. Uhlmann, An immersed boundary method with direct forcing for the simulation of particulate flows, Journal of Computational Physics 209 (2) (2005) 448476.
[8] K. Taira, T. Colonius, The immersed boundary method: A projection approach, Journal of Computational Physics 225 (2) (2007) 21182137.
[9] A. Pinelli, I. Naqavi, U. Piomelli, J. Favier, Immersed-boundary methods for general finite-difference and finite-volume Navier-Stokes solvers, Journal of Computational Physics 229 (24) (2010) 90739091.
[10] T. Kempe, J. Frhlich, An improved immersed boundary method with direct forcing for the simulation of particle laden flows, Journal of Computational Physics 231 (9) (2012) 36633684.

[11] D. Le, B. Khoo, K. Lim, An implicit-forcing immersed boundary method for simulating viscous flows in irregular domains, Computer Methods in Applied Mechanics and Engineering 197 (2528) (2008) 21192130.
[12] J. Wu, C. Shu, Implicit velocity correction-based immersed boundary-lattice boltzmann method and its applications, Journal of Computational Physics 228 (6) (2009) 1963–1979.
[13] S. Gsell, U. D'Ortona, J. Favier, Explicit and viscosity-independent immersed-boundary scheme for the lattice Boltzmann method, Physical Review E 100 (3) (2019) 033306.
[14] S. Gsell, U. D'Ortona, J. Favier, Multigrid dual-time-stepping lattice Boltzmann method, Physical Review E 101 (2) (2020) 023309.
[15] R. Bourguet, D. Lo Jacono, Flow-induced vibrations of a rotating cylinder, Journal of Fluid Mechanics 740 (2014) 342380.
[16] D. Stojković, M. Breuer, F. Durst, Effect of high rotation rates on the laminar flow around a circular cylinder, Physics of fluids 14 (9) (2002) 3160–3178.